The Astrophysical Journal, 886:39 (17pp), 2019 November 20 https://doi.org/10.3847/1538-4357/ab4a14

Toward a More Complex Description of Chemical Profiles in Exoplanet Retrievals: A Two-layer Parameterization

Q. Changeat, B. Edwards, I. P. Waldmann, and G. Tinetti
Department of Physics and Astronomy, University College London, Gower Street, WC1E 6BT London, UK; quentin.changeat.18@ucl.ac.uk
Received 2019 March 26; revised 2019 September 29; accepted 2019 September 29; published 2019 November 18

Abstract

State of the art spectral retrieval models of exoplanet atmospheres assume constant chemical profiles with altitude. This assumption is justified by the information content of current data sets which do not allow, in most cases, for the molecular abundances as a function of pressure to be constrained. In the context of the next generation of telescopes, a more accurate description of chemical profiles may become crucial to interpret observations and gain new insights into atmospheric physics. We explore here the possibility of retrieving pressure-dependent chemical profiles from transit spectra, without injecting any priors from theoretical chemical models in our retrievals. The "two-layer" parameterization presented here allows for the independent extraction of molecular abundances above and below a certain atmospheric pressure. By simulating various cases, we demonstrate that this evolution from constant chemical abundances is justified by the information content of spectra provided by future space instruments. Comparisons with traditional retrieval models show that assumptions made on chemical profiles may significantly impact retrieved parameters, such as the atmospheric temperature, and justify the attention we give here to this issue. We find that the two-layer retrieval accurately captures discontinuities in the vertical chemical profiles, which could be caused by disequilibrium processes—such as photochemistry—or the presence of clouds/hazes. The two-layer retrieval could also help to constrain the composition of clouds and hazes by exploring the correlation between the chemical changes in the gaseous phase and the pressure at which the condensed phase occurs. The two-layer retrieval presented here therefore represents an important step forward in our ability to constrain theoretical chemical models and cloud/haze composition from the analysis of future observations.

Key words: planets and satellites: atmospheres – techniques: spectroscopic

1. Introduction

In the past years an increasing number of exoplanetary atmospheres have been characterized with space- and ground-based observatories. Ultraviolet, optical, and infrared spectra, recorded through transit, eclipse, high-dispersion, and direct imaging, have offered a glimpse of the atmospheric structure and composition of exotic worlds orbiting other stars. In most cases the data available are sparse and therefore their interpretation is rarely unique. To explore the degeneracy, reliability, and correlations among the atmospheric parameters extracted from the data, the past decade has seen a surge in spectral retrieval models developed by many teams (e.g., Terrile et al. 2005; Irwin et al. 2008; Madhusudhan & Seager 2009; Line et al. 2013; Waldmann et al. 2015b; Cubillos et al. 2016; Lavie 2017; Gandhi & Madhusudhan 2018; Goyal et al. 2018).

Most current spectral retrieval models assume constant or simplified atmospheric thermal profiles. Additionally, chemical profiles which are constant with altitude are assumed (e.g., MacDonald & Madhusudhan 2017; Tsiaras et al. 2018; Pinhas et al. 2019). In these models, the mixing ratio of each individual molecule is fully determined by a single free parameter. So far, this approach has been successful due to the relatively poor quality of the input data from space- and ground-based instruments. Given the low signal-to-noise, spectral resolution, and the narrow wavelength coverage, current data cannot be used to constrain more complex models. However, the next generation of telescopes coming online in the next decade will demand more complex retrievals to extract all the information content embedded in the data. In the context of NASA-*James Webb Space Telescope* (*JWST*; Bean et al. 2018), ESA-*ARIEL* (Tinetti et al. 2018), and other facilities from ground and space (e.g., E-ELT (Brandl et al. 2018), Twinkle (Edwards et al. 2019b)), with higher resolution, signal-to-noise ratio (S/N), and broader wavelength range, will allow for less abundant trace gases and refined thermal profiles to be captured. For instance, Rocchetto et al. (2016) have demonstrated that the assumption of constant atmospheric thermal profiles will be inadequate to correctly interpret future better-quality transit spectra recorded from space. Additionally, these new instruments may be sensitive enough to constrain nonconstant chemical profiles.

The need for increased chemical complexity is sometimes addressed in the literature through additional constraints in the retrievals from dynamical and chemical models ("hybrid" models). This method is already widely explored in retrievals aiming at constraining the thermal profiles, e.g., the Guillot model (Guillot 2010) and other two-stream approximations (Heng et al. 2014; Malik et al. 2017). This strategy allows for more complex thermal profiles to be considered, while limiting the number of free parameters. Similarly, equilibrium and disequilibrium chemical models may be used to constrain chemical profiles. Agúndez et al. (2014) showed, with their 2D chemical model of HD 209458b and HD 189733b, that accurate parameterizations of exoplanetary atmospheres could be extremely complex. Interesting alternatives combine both physical/chemical models and free parameters such as the

model adopted by Madhusudhan & Seager (2009), where the chemical profiles are computed in equilibrium and multiplied by a factor to account for potential departures from the equilibrium.

The hybrid retrieval models have, however, two major disadvantages. First, the forward model requires significant computing time to ensure convergence of the chemical/dynamical modules, which becomes even longer if used for retrievals. More fundamentally, they imply assumptions on the state of the planet and its physical/chemical behavior. As the physics of such systems can be extremely complex and far from any environment we know in the solar system, the selection of a particular model may lead to results biased by preconception. For instance, Venot et al. (2012) proposed a disequilibrium model adapted for hot-Jupiters and found significant differences when comparing with other models such as the equilibrium ones. This result highlights the issue of assuming a particular physics as a prior in inverse models, when our knowledge of exoplanetary atmospheres is still in an early phase. At least until our knowledge of these exotic worlds has progressed substantially, the results obtained by spectral retrievals should be kept independent from ab initio dynamical and chemical models, and used instead to constrain/validate some aspects of said models.

The approach taken here is to increase the number of free variables for each molecular species considered. Applying this approach to currently available data is not justifiable as it would simply increase the degeneracy of the retrieved solutions. By contrast, attempts to use models of inadequate complexity to analyze spectra observed by next generation facilities are likely to provide incomplete pictures and misleading results. This paper explores the importance of moving toward a more complete description of chemical profiles through the analysis of simulated transit data from *JWST*, *ARIEL*, and other future telescopes. In that context, we consider the example of a two-layer parameterization with three degrees of freedom.

Section 2 presents the two-layer approach and describes the methodology adopted. A validation of the method using simple cases is then reported in Section 3, followed by specific examples of exoplanetary atmospheres in Section 4. Section 5 discusses the model's strengths and limitations.

2. Methodology

2.1. Overview and Key Assumptions

This work focuses on retrievals of transit spectra, so that, for simplicity, the thermal profile can be assumed isothermal in some benchmark cases—note that this assumption is abandoned in Section 4 to ensure our simulations are as realistic as possible. In eclipse spectroscopy, the thermal gradients and the chemical profiles are always entangled, making it a more complex case which will be considered in a separate paper.

The two-layer parameterization has been adopted for its simplicity and because it does not rely on external physical assumptions which, as previously described, could bias the results of the retrieval. While our model is clearly not representative of all real atmospheres, it allows us to consider a departure from the constant mixing ratios case.

Both the forward radiative transfer models and the inverse models (spectral retrievals) are based on the open-source TauREx from Waldmann et al. (2015a, 2015b), which has been modified for the purpose of this study. TauREx is a fully Bayesian radiative transfer and retrieval framework that encompasses molecular line lists from the Exomol project (Tennyson et al. 2016), HITEMP (Rothman & Gordon 2014), and HITRAN (Gordon et al. 2016). The complete list of opacity used in this paper can be found in Table 1. The public version of TauREx[1] is able to retrieve chemical composition of exoplanets by assuming constant abundances with altitude. It can also simulate atmospheres in equilibrium.

Table 1
List of Opacities Used in This Work

Opacity	References
H_2–H_2	Abel et al. (2011), Fletcher et al. (2018)
H_2–He	Abel et al. (2012)
H_2O	Barton et al. (2017), Polyansky et al. (2018)
CH_4	Hill et al. (2013), Yurchenko & Tennyson (2014)
CO	Li et al. (2015)
CO_2	Rothman et al. (2010)
TiO	Schwenke (1998)

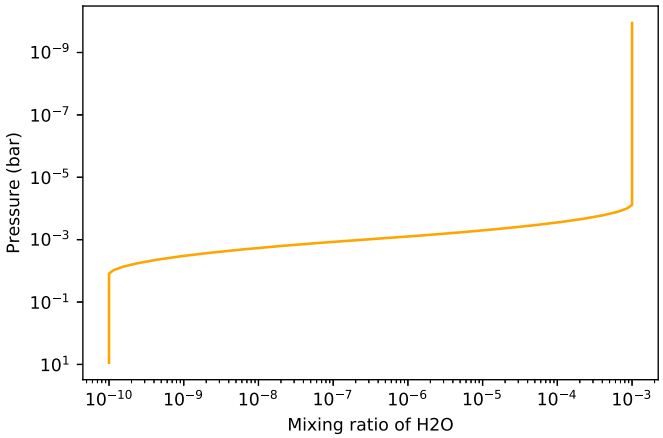

Figure 1. Example of a two-layer chemical profile with H_2O. This profile can be used as input for forward simulations of exoplanet spectra, as well as for fitting data in retrievals. Here, the surface layer is depleted with a mixing ratio $X_S(H_2O)$ of 10^{-10} and the top layer has a large quantity of H_2O, with $X_T(H_2O) = 10^{-3}$. The separation pressure of the two layers is set to $_{PI}(H_2O) = 10^{-3}$ bar and the transition is smoothed over 10% of the atmosphere (10 layers).

Here we added the new two-layer module to the code. The chemical parameterization we used can be described by three variables: the surface/bottom abundance X_S, the top abundance X_T, and the pressure defining the separation of the two layers (input pressure point P_I for the forward model and retrieved pressure point P_R). The chemical profile is linearly interpolated in log space—smoothing over 10% of the atmosphere—to avoid a sharp transition in the profile. An example of a two-layer chemical profile for water vapor is given in Figure 1.

For all the tests reported in this paper, we follow the three-step procedure detailed below.

2.2. Step 1: Generating High-resolution Input Spectra

We start by using TauREx in forward mode and generate a high-resolution theoretical spectrum. In our models, we assumed a maximum pressure of 10 bar, corresponding to the planet surface. The atmosphere is composed of the inactive gases H_2 and He, for which we set the ratio He/H_2 to 0.15 and

[1] https://github.com/ucl-exoplanets/TauREx_public

Table 2
Interpretation of the Bayes ratio (Kass & Raftery 1995)

log(*B*)	Interpretation
0–0.5	No Evidence
0.5–1	Some Evidence
1–2	Strong Evidence
>2	Decisive

add the considered active molecules (relative abundance defined by their mixing ratio). We consider collision induced absorption of the H_2–H_2 and H_2–He pairs and opacities induced by Rayleigh scattering (Cox 2015). Throughout the paper, the molecular mixing ratios and profiles in the forward model are varied to create high resolution spectra for a wide range of compositions and cases. The planetary parameters have been set to the well known exoplanet HD 209458b in Section 3 and are listed in the Appendix. The adopted approach is compatible with any other set of planetary and atmospheric parameters and is applied in Section 4 to two other simulated planets inspired by WASP-33 b and GJ 1214b.

2.3. Step 2: Convolution of the Input Spectra with the Instrument Response Function

High-resolution theoretical spectra obtained in Section 2.2 are convolved with the instrument response function to simulate realistic observations. We use ArielRad (L. Mugnai et al. 2019, in preparation) to provide realistic noise models for spectra obtained by *ARIEL* and chose planets that are in the current target list (Edwards et al. 2019a). In the case of *JWST*, we used the noise estimates for HD 209458b presented in Rocchetto et al. (2016). An example of this process is shown in Figure 2 where both the high-resolution theoretical spectrum and the *ARIEL*-simulated case are presented.

2.4. Step 3: Retrievals

We run TauREx in retrieval mode and use the spectra obtained in step 2 as input to the retrieval. We used the nested sampling algorithm Multinest from Feroz et al. (2009) with 1500 live points and a log likelihood tolerance of 0.5. The retrieved parameters include our chemical setup (three variables per chemical species), the isothermal temperature value and the planet radius. We therefore have a minimum of five free parameters that we attempt to retrieve. In the case where the mixing ratios were assumed constant with altitude (one-layer forward model), the retrieved pressure point has been fixed, so that we have only two free variables per chemical species or a minimum of four free parameters. In our retrieval scheme, we use uniform priors for all the free parameters. In all our retrievals, chemical abundances are allowed to explore the bounds 10^{-12} to 10^{-1}. For the retrieved pressure point, we allow the bounds from 10^{-1} to 10^{-4} bar for the Section 3. In Section 4, since we investigate less ad hoc situations, we allow the pressure to explore 10^{-1} to 10^{-7} bar. For the isothermal temperature retrievals, the priors span ±30% of the ground truth value. In Section 4, since we investigate more realistic examples, we retrieve a three-point temperature profile (Waldmann et al. 2015a). The atmospheric parameters used to generate the theoretical spectrum in step 1 are the ground truth. By comparing the posteriors obtained by the retrieval to the ground truth, we can test the reliability and accuracy of the retrieval process.

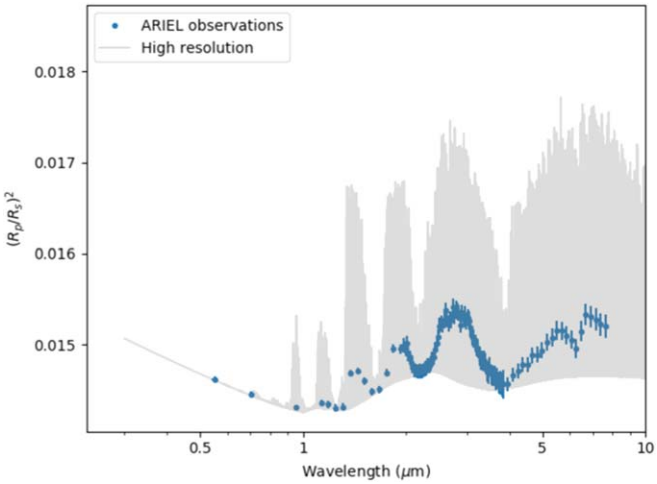

Figure 2. Example of forward models assuming a two-layer chemical profile of H_2O as shown in Figure 1. Gray curve: high-resolution theoretical spectrum obtained with TauREx at step 1 (Section 2.2). Blue curve: simulated *ARIEL* observations after having processed the theoretical spectrum in step 2 (Section 2.3).

Furthermore, by using the predicted performances of *JWST* and *ARIEL*, we can quantify the expected information content of future data, with a view to assessing the ability to probe the chemical complexity of exoplanet atmospheres. For each retrieval, we state the nested sampling log-evidence. Bayes factor B (Jeffreys 1998), which is the ratio of the evidences of two competing models (E_1 and E_2), allows us to compare models against each other. In practice, the table in Kass & Raftery (1995) gives an interpretation of $\log(B) = \Delta\log(E) = \log(E_2) - \log(E_1)$ (see Table 2).

By applying the three-step methodology, a number of cases are simulated. First, we verify that the two-layer retrieval is able to recover the more basic one-layer input (i.e., a constant chemical profile). We then investigate the "retrievability" of the two-layer input spectrum by a two-layer retrieval in the case of *JWST* and *ARIEL* observations. Finally, we explore the advantage of using a two-layer approach by comparing how a two-layer input spectrum is recovered by both one- and two-layer retrievals.

2.5. Testing the Two-layer Approach: Retrieval of a One-layer Input Spectrum Using the Two-layer Parameterization

As a sanity check, we test that the more complex two-layer model can indeed recognize the simple case of constant chemistry. A one-layer simulated spectrum is generated and we attempt to recover the solution using the two-layer model. Here, the retrieval of the pressure point (P_R) is disabled as this parameter introduces intrinsic degeneracy in the specific case of constant chemistry. Here, the goal being to illustrate that our two-layer model returns the expected solution when tested on the one-layer forward model, the behavior of the retrieval when the retrieved pressure point is activated is discussed in Section 4. As any value for this point would work, we arbitrarily choose to set it at $P_I = 10^{-1.3}$ bar.

2.6. Retrieval of a Two-layer Input Spectrum as Observed by JWST *and* ARIEL

We study an exoplanet exhibiting noticeable chemical modulations with altitude. This case can be simulated by using

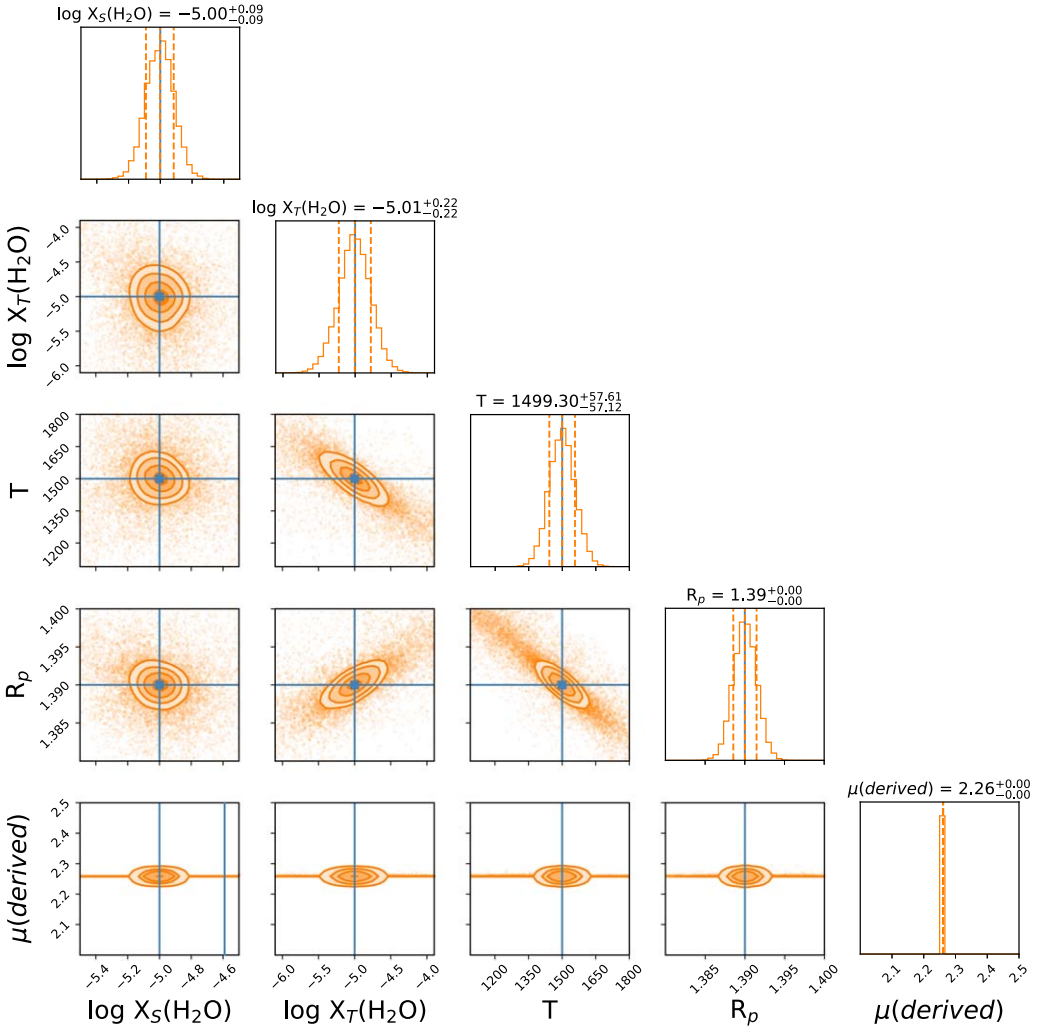

Figure 3. Posterior distributions of a one-layer input atmosphere retrieved using the two-layer model. The input spectrum was generated by assuming a constant profile for H_2O with a mixing ratio of 10^{-5}. In this example, the retrieved pressure point is disabled and arbitrarily set at $_{P_l = 10^{-1.3}}$ bar. For each free parameter, we report the mean and 1σ iso likelihood levels with the dashed lines. The retrieved values match the input values within the retrieved uncertainties.

a two-layer profile as input. We present the particular case of an input H_2O profile with two layers separating at $P_l(H_2O) = 10^{-2}$ bar. The input H_2O surface layer is set with a mixing ratio of $X_S(H_2O) = 10^{-3}$ and the top layer contains $X_T(H_2O) = 10^{-5}$. The input spectrum is simulated at high-resolution and observations are reproduced by convolving the theoretical spectrum to the instrument response function of *JWST* and *ARIEL*.

2.7. Comparison of the One-layer and Two-layer Retrievals.

By comparing the results obtained with the one-layer and two-layer retrievals, we aim to illustrate issues that may occur when performing a retrieval with a model of inappropriate complexity. Therefore, we simulate planetary atmospheres with two-layer chemical profiles and analyze the results if the retrieval is performed with a one-layer chemical approach. For this test, we use *ARIEL* simulations to illustrate our results. In particular, two main issues could occur and need to be tested:

1. The observed spectrum cannot be explained using the one-layer retrieval, as the best solution retrieved does not fit the data.
2. The one-layer retrieval manages to achieve a "good" fit but the retrieved parameters are wrong compared to the ground truth. This issue is more subtle as there is little evidence and no direct way to spot the error.

These two points can be tested by considering the following examples. For the former, we assume an atmosphere with a single CH_4 profile with a surface layer of $X_S(CH_4) = 10^{-5}$ up to $P_l(CH_4) = 10^{-2}$ bar and $X_T(CH_4) = 10^{-10}$ above that pressure, corresponding to a depleted layer. For the latter, we simulate a single H_2O profile where the planet contains $X_S(H_2O) = 10^{-10}$ up to 10^{-2} bar and the mixing ratio is $X_T(H_2O) = 10^{-3}$ for lower pressures.

3. Results

3.1. Testing the Two-layer Approach: Retrieval of a One-layer Input Spectrum Using the Two-layer Parameterization

The retrieved posterior distributions for an input spectrum generated with one-layer parameterization with a single species, H_2O, is presented in Figure 3. In orange, we show the retrieved posterior distribution of the parameters, while the true value (when available) is marked in blue. The mixing ratio of H_2O used for this example was 10^{-5}. The two-layer model

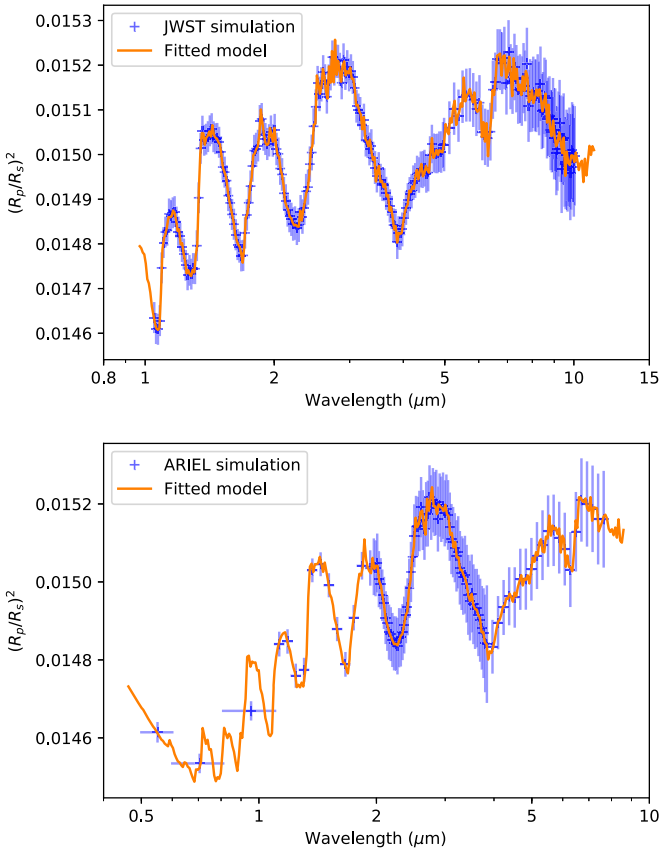

Figure 4. Retrieved spectra for a hot-Jupiter similar to HD 209458b which presents a two-layer H_2O chemical profile. Case without Gaussian scatter added to the data points. Top: *JWST* simulated performance ($\log(E) = 2076$); bottom: *ARIEL* simulated performance ($\log(E) = 883$).

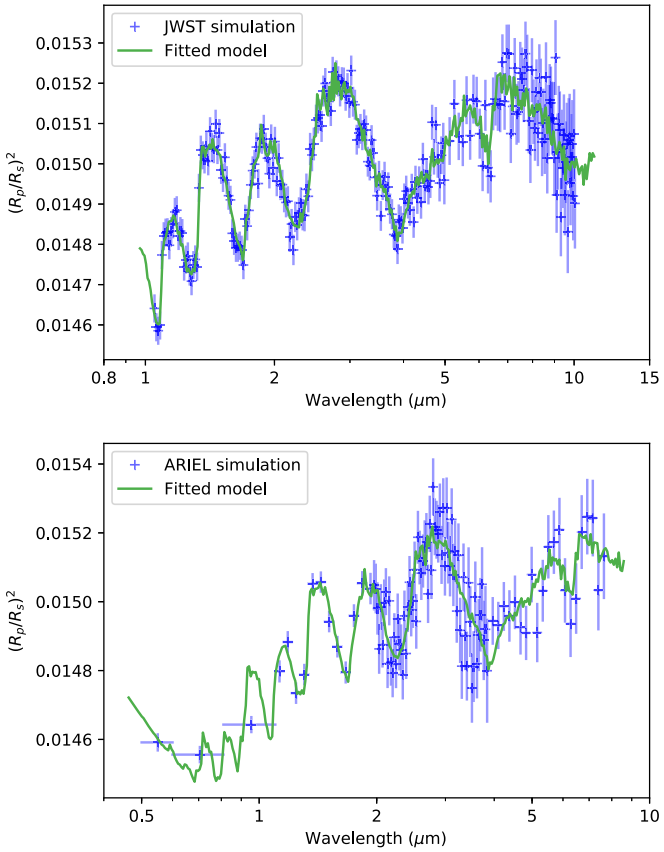

Figure 5. Retrieved spectra for a hot-Jupiter similar to HD 209458b with a two-layer H_2O chemical profile. Gaussian scatter was added to the mean data points. Top: *JWST* simulated performance ($\log(E) = 1985$); bottom: *ARIEL* simulated performance ($\log(E) = 828$).

successfully retrieved the same abundance for both layers. This result matches the single input parameter and confirms that the two-layer parameterization can recover the one-layer input. This example showcases a situation where the complexity of the retrieval model is higher than the input.

3.2. Retrieval of a Two-layer Input Spectrum As Observed By JWST *and* ARIEL

The input H_2O surface layer was set as $X_S(H_2O) = 10^{-3}$ and the top layer contained $X_T(H_2O) = 10^{-5}$. These abundances result in strong features in the spectrum but additional retrievals show that similar conclusions can be obtained for mixing ratios down to 10^{-6} and for other molecules. The limits of the model are discussed in Section 5. The planet parameters are retrieved for *JWST* and *ARIEL* using the two-layer model. The best fitted spectra are presented in Figure 4 for the two telescopes. We also run the same cases with the noised up spectra, where we applied a dispersion corresponding to the uncertainties (see Figure 5). We show the posterior distributions of both cases for the *JWST* and *ARIEL* simulations in Figure 6.

The model is able to recognize the two layers in *ARIEL* and *JWST* simulations for the scattered and nonscattered cases.

Typically, to simulate an observation instance, the flux per wavelength observed, F_λ, is drawn from a Gaussian distribution (in the limit of N_{photons} being large) defined by its 1σ error bar and the "noise-free" mean flux of the forward model, $\bar{F}_\lambda$. Here, we decided not to sample from this distribution and to adopt the "noise-free" mean for the following reason. In this publication we are interested in the intrinsic biases resulting from using oversimplified to more complex (one-layer versus two-layer) chemical profiles. To study these biases, one can either generate thousands of noise instances, N_{instance} and average their retrieval results to obtain the underlying mean of the distribution, or avoid adding noise to $\bar{F}_\lambda$ in the first place. Given that in this case, all noise is normally distributed and following the central-limit theorem (in the limit of large N_{instance}) both approaches are equivalent. Feng et al. (2018) showed this to be the case and adopted the same rationale in their study. For the rest of the paper we therefore do not scatter our simulated spectra.

In the *ARIEL* case, we accurately retrieved both the surface layer ($X_S(H_2O) = 10^{-2.97}$) and the top layer ($X_T(H_2O) = 10^{-5.12}$). The Retrieved Pressure Point also matched the input parameters ($P_R(H_2O) = 10^{-2.06}$ bar). The same conclusions are reached for *JWST*. Additionally, in both simulations, the two-layer retrievals recovered the correct temperature of 1500 K and radius (1.39 R_J) corresponding to the input.

3.3. Comparison Between the One-layer and Two-layer Retrievals

We show here the results of the test where the input spectrum was generated assuming CH_4 only with $X_S(CH_4) = 10^{-5}$ up to $P_t(CH_4) = 10^{-2}$ bar and $X_T(CH_4) = 10^{-10}$. $X_T(CH_4) = 10^{-10}$ does not produce any observable feature, so for this layer we expect to retrieve only an upper limit in the posteriors. In this example, the one-layer retrieval has

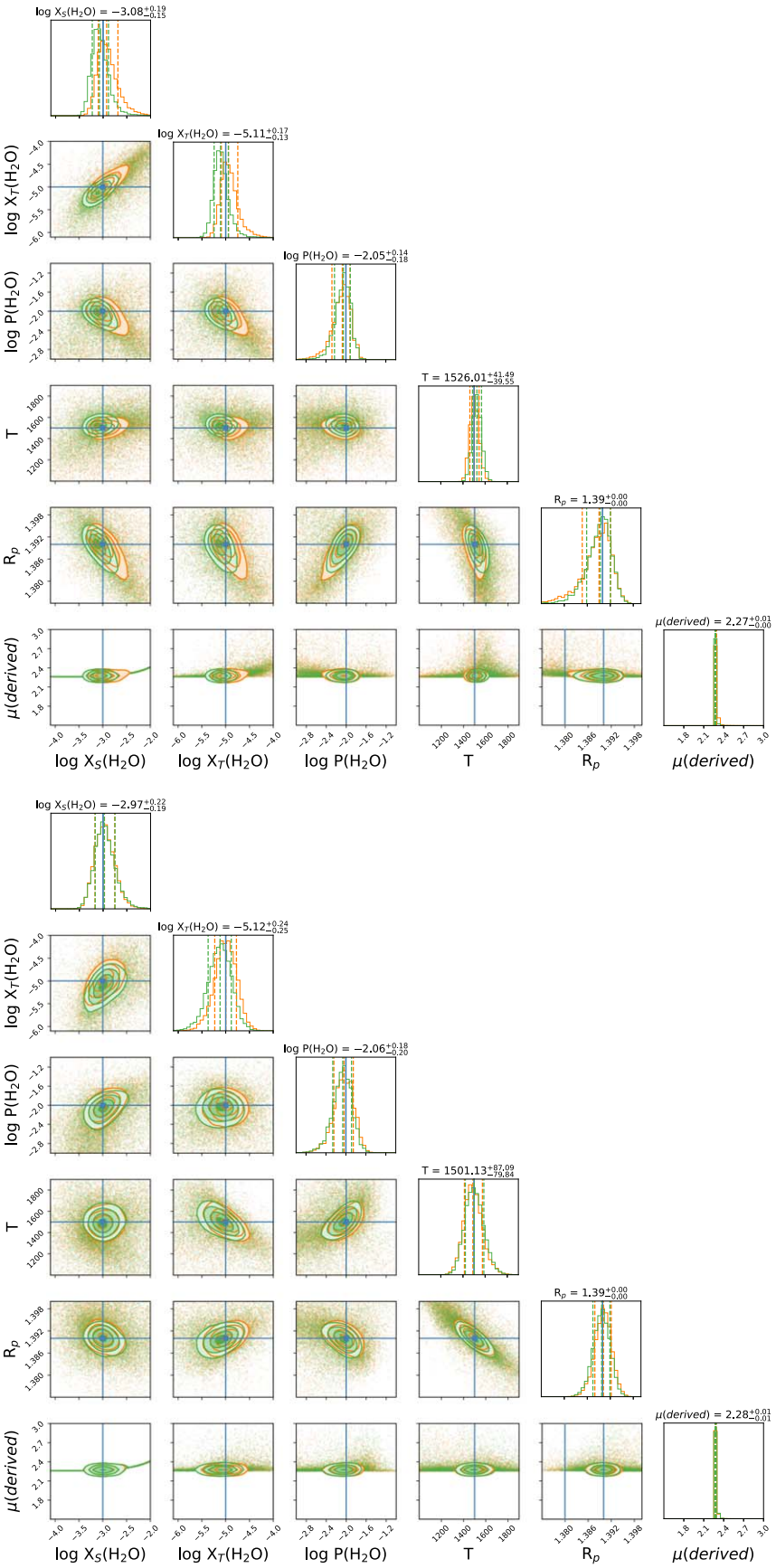

Figure 6. Posterior distributions of the *JWST* and *ARIEL* simulations (Figures 4 and 5) for a hot-Jupiter similar to HD 209458b, which presents a two-layer H_2O chemical profile. The input atmosphere contains $X_S(H_2O) = 10^{-3}$ for the bottom layer and $X_T(H_2O) = 10^{-5}$ for the top layer of the atmosphere. The layer's separation is set at $P(H_2O) = 10^{-2}$ bar and the retrieval is performed with the two-layer model. In both the *JWST* and *ARIEL* retrievals, all chemical variables are well retrieved. Top: *JWST*; bottom: *ARIEL*. The orange posteriors correspond to the case without noise, while the green ones are for the noisy cases.

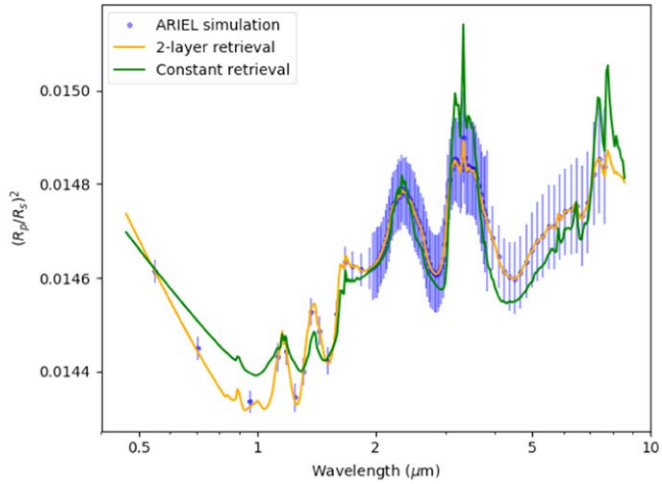

Figure 7. Observed input spectrum obtained with a two-layer CH_4 profile and retrieved spectrum obtained with a one-layer retrieval. This example showcases that the one-layer retrieval is inadequate to interpret the data. The correct two-layer retrieval is also shown. The nested sampling global evidence is log $(E) = 737$ for the one-layer and $\log(E) = 885$ for the two-layer retrieval. This implies $\log(B) = 148$, which is decisively in favor of the two-layer scenario.

difficulties in fitting the observed spectrum, as shown in Figure 7. In this case, the one-layer retrieval lacks flexibility, which leads to a poor fit of the spectrum. This is also backed up by the lower nested sampling global evidence for the one-layer scenario: 737 for the one-layer and 885 for the two-layer ($\Delta\log(E) = 148$). This example illustrates the need for a two-layer retrieval.

Concerning the test where the input spectrum was generated with H_2O only and assuming $X_S(H_2O) = 10^{-10}$ and $X_T(H_2O) = 10^{-3}$ above 10^{-2} bar, both the one-layer and two-layer retrievals converged to a solution and gave satisfactory fits of the input spectrum (see Figure 9). The posterior distributions are presented in Appendix B, Figure 14. Unsurprisingly, the two-layer retrieval managed to recover the correct input parameters. However, while fitting the spectrum, significant differences appear for the one-layer model in the retrieved parameters. The one-layer retrieval tries to compensate for the lack of flexibility in the chemical profile by increasing the temperature to 2100 K instead of the 1500 K ground truth temperature. The input chemical and thermal profiles for both retrievals are shown in Figure 8.

The retrieved temperature by the one-layer retrieval is significantly off compared to the input, while the retrieved H_2O mixing ratio approximates the atmospheric average. This example illustrates well the importance of exploring and understanding more complex chemical models in retrievals. Here the retrieved spectrum using the one-layer approximation (Figure 9) gives an acceptable fit while leading to a wrong solution, which is a serious issue. Small differences compared to the observations are noticeable which, in this case, would still permit the selection of the two-layer solution, provided that both retrievals are performed. More importantly, the correct solution can be determined by comparing the nested sampling global log-evidence of the retrieval. The two-layer retrieval obtained a value of $\log(E) = 883$ while the one-layer only had $\log(E) = 733$, indicating a clear preference for the two-layer scenario (difference of $\Delta\log(E) = 150$).

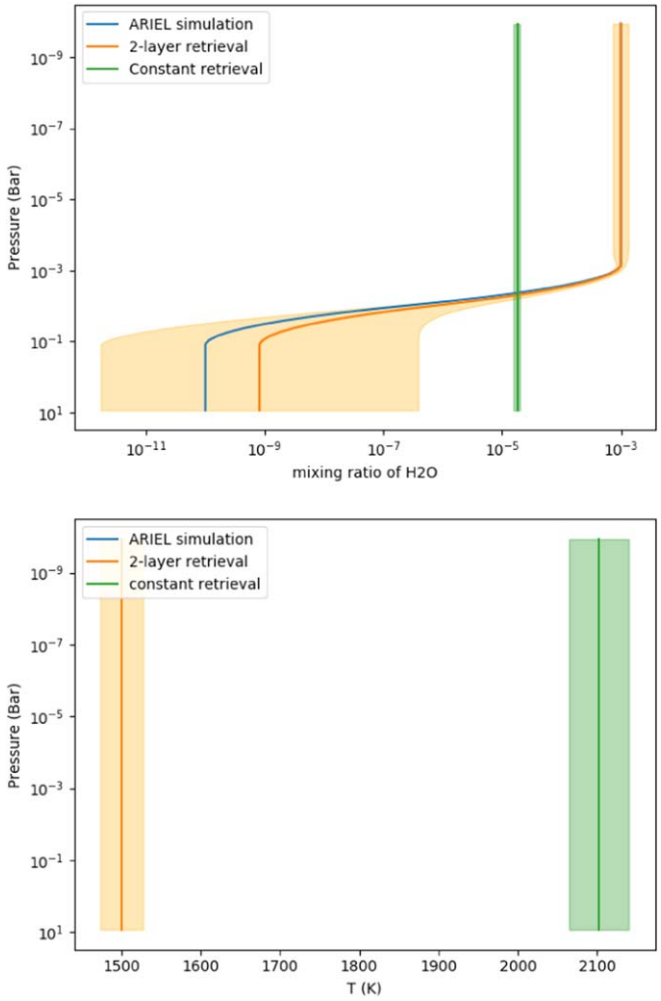

Figure 8. Chemical (top) and temperature (bottom) profiles for the input atmospheric model, the two-layer and one-layer retrievals. For the temperature, the one-layer model is strongly biased. The input model temperature is not clearly visible as it overlaps with the retrieved value of the two-layer retrieval at 1500 K.

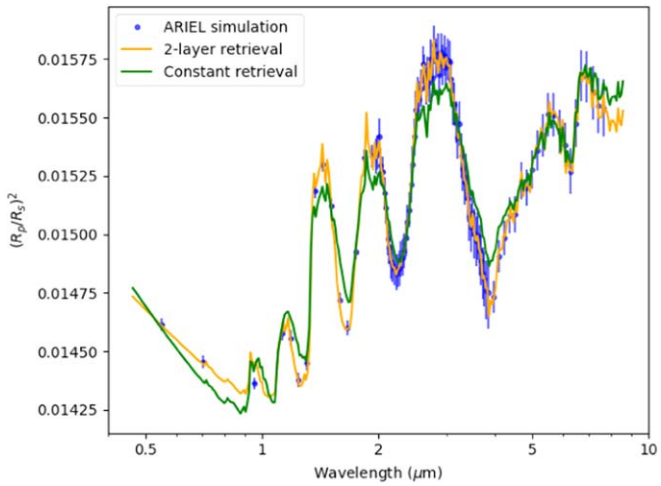

Figure 9. Observed spectrum generated with a two-layer H_2O profile as input and best retrieved solutions obtained with one-layer and two-layer retrievals. While the two-layer retrieval captures the observations better, the differences with the one-layer fit are relatively small. The nested sampling global evidence is $\log(E) = 733$ for the one-layer and $\log(E) = 883$ for the two-layer retrieval.

4. More Realistic Examples

The previous sections demonstrated the theoretical possibility and, in some cases, the necessity of retrieving two-layer chemical profiles in a number of select, simplified examples. Here we test the two-layer approach by applying it to two cases inspired by GJ 1214b and WASP-33 b. Spectra and parameters used in this section should not be considered as the "true" values of these real planets: they are realistic scenarios inspired from examples of the literature, which are here used to explore advantages and limitations of the two-layer approach.

For instance, recent observations of the sub-Neptune GJ 1214b in the near-IR unveiled a featureless spectrum, which could be caused by high-altitude hazes. Also, recent observations of the ultra hot-Jupiter WASP-33 b point toward a thermal inversion and a significant amount of TiO, which could cause this inversion by acting as a strong absorber in the visible. We simulate the WASP-33 b case with a two-layer input model, while in the GJ 1214 b case we highlight the pertinence of our model by using the profiles from a disequilibrium chemistry model as input. We detail below all the assumptions we considered for our tests.

4.1. An Ultra Hot-Jupiter Inspired by WASP-33 b

Current analyses of ground- and space-based observations of WASP-33 b suggest extreme temperatures reaching 3800 K and a possible thermal inversion in the atmosphere (Haynes et al. 2015; Nugroho et al. 2017). TiO or VO, which are strong absorbers at short wavelengths, could very efficiently capture high-energy stellar photons at the top of the atmosphere and cause the inversion (Fortney et al. 2008; Spiegel et al. 2009). In parallel, other observations have suggested the presence of TiO in WASP-121 b (Evans et al. 2017) and WASP-76 b (Tsiaras et al. 2018).

Here we investigate this process by attempting to detect a TiO layer in the upper atmosphere of a simulated planet resembling WASP-33 b. Our input model includes only two molecules: H_2O and TiO. The simulation consists of a constant mixing ratio of 10^{-4} for H_2O and an inverted temperature-pressure (TP) profile from 2800 to 3700 K, which is inspired by Haynes et al. (2015). For the temperature-pressure profile we used a three-point model (Waldmann et al. 2015a). This model interpolates a smooth TP profile using five free parameters, i.e., surface temperature and two TP points. The temperature variations allow us to explore the possibility of retrieving both thermal and chemical parametric profiles at the same time. Rocchetto et al. (2016) have shown that nonisothermal profiles could introduce a bias in *JWST* observations. This is also expected to be true for *ARIEL* and we can investigate it as a side result of this work. For the retrieval, we explore uniform priors on the pressure bounds 10^{-2}–10^{1} bar for the point 1 and 10^{-5}–10^{-1} bar for the point 2. The temperature bounds are the same for all three retrieved points and cover a range 30% lower/higher than the input min/max temperatures (1960–4690 K). For a real observation, these priors could be informed by the knowledge of the equilibrium temperature and the physics of the atmosphere. To simulate a stratospheric TiO layer, we assumed abundances of $X_I(\mathrm{TiO}) = 10^{-4}$ for the top layer (down to $P_I = 10^{-4}$ bar) and $X_S(\mathrm{TiO}) = 10^{-7}$ at the surface. The spectrum, as well as the temperature and chemical profiles, are presented in Figure 10 while the full posterior distribution is available in the Appendix C, Figure 15.

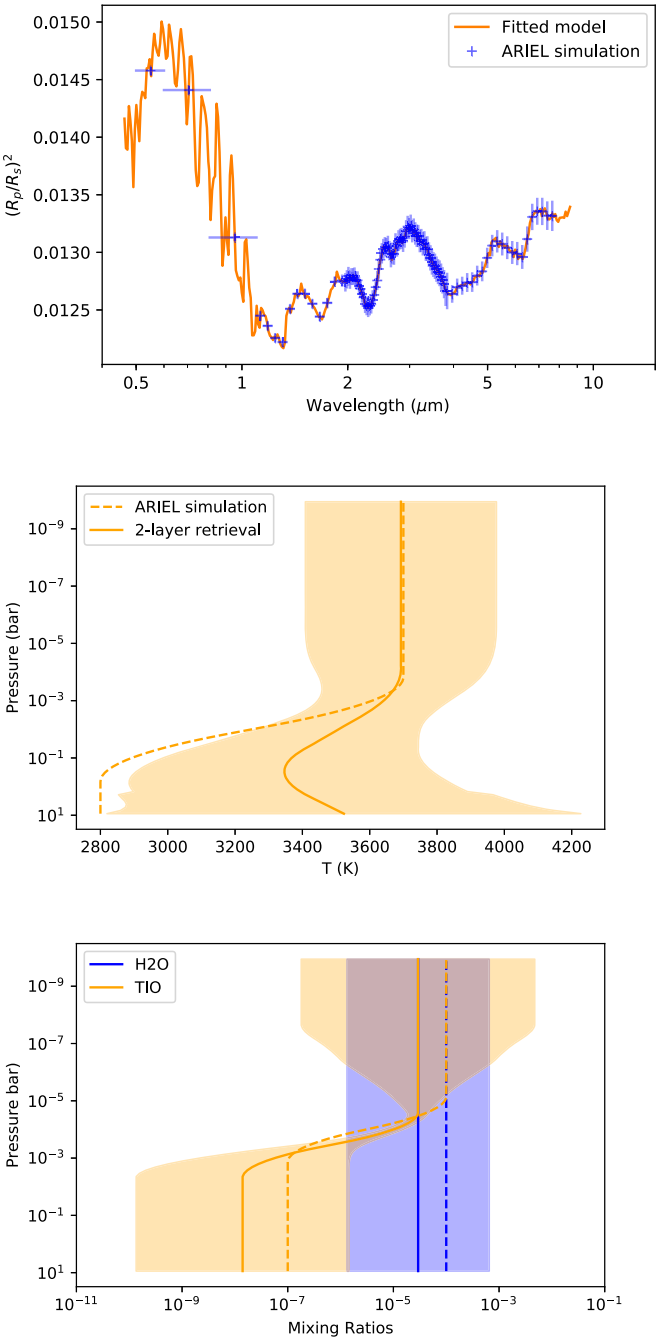

Figure 10. Outcome of the WASP-33 b retrieval simulations. Top: fitted spectrum; middle: retrieved temperature profile; bottom: retrieved chemical profiles of H_2O and TiO. The dashed lines correspond to the input values assumed in the forward model while the solid lines indicate the retrieved profiles. For this run $\log(E) = 880$.

These results demonstrate the possibility of accurately retrieving the vertical distribution of the TiO layer. In particular, the TiO profile is well constrained between 10^{-6} and 10^{-3} bar as a result of the strong features between 0.4 and 1 μm. The shape of the thermal profile is also correctly retrieved, although with a larger uncertainty at higher pressures as shown by the posterior distribution. The retrievability of the thermal and chemical profiles at the same time indicates that retrievals of future transit spectra should take these two effects into account. The flexibility of the two-layer approach allows for the confirmation (or rejection) of potential correlations

between molecules/condensates and thermal inversions. This is an important application of the two-layer approach.

4.2. A Warm Sub-Neptune Inspired by GJ 1214b

As previously mentioned, GJ 1214b is a sub-Neptune with a relatively flat spectrum in the visible and near-infrared. Multiple explanations for the lack of features have been proposed (Miller-Ricci Kempton et al. 2012; Morley et al. 2013; Kreidberg et al. 2014):

1. The planet could have an atmosphere heavier than hydrogen, such as a water dominated atmosphere.
2. The atmosphere could be hydrogen dominated with opaque, high altitude clouds (e.g., KCl or ZnS).
3. The planet could have hydrocarbon hazes in the upper atmosphere.

Here we investigate the retrievability of the third scenario as an example of two-layer chemistry. The photochemical hazes could be similar to those found in the atmosphere of Saturn's moon Titan. CH_4 in the upper atmosphere is photolyzed by radiation, creating hydrocarbon hazes that are opaque in the near-infrared. This scenario implies a significant CH_4 abundance at the surface of the atmosphere and a sharp decline in the upper atmosphere. For our input forward model, we used the chemical profiles of the four molecules H_2O, CH_4, CO_2, and CO published by Miller-Ricci Kempton et al. (2012) in the case of solar abundance and $Kzz = 10^6$ cm^2 s^{-1}. The profiles are retrieved using two scenarios: a hybrid one with two-layer chemistry for H_2O and CH_4 and the one-layer for CO_2 and CO; and a fully one-layer chemistry with all four molecules retrieved using constant profiles. For the hybrid case, the abundances of CO_2 and CO were indeed too low to retrieve the two-layer profile. The other input parameters for the planet are described in the Appendix. We add a hydrocarbon hazes layer adopting the model described in Lee et al. (2013). The clouds are treated as additional opacity σ_c for each layer of size Δz:

$$\sigma_c = Q_{\rm ext}\,\pi R_{\rm clouds}^2\,\chi_{\rm clouds}\,\Delta z. \quad (1)$$

Where $R_{\rm clouds}$ is the size of the cloud particles and $\chi_{\rm clouds}$ is the cloud number density. Here the extinction efficiency $Q_{\rm ext}$ has been defined as:

$$Q_{\rm ext} = \frac{5}{Q_0 x^{-4} + x^{0.2}}, \quad (2)$$

and the cloud size parameter x is:

$$x = \frac{2\pi R_{\rm clouds}}{\lambda}. \quad (3)$$

In the forward model, the particle size $R_{\rm clouds}$ was assumed to be 0.01 μm while $\chi_{\rm clouds}$ was set to 10^{-6}. We also simplify our problem by assuming the hazes cover the entire atmospheric pressure range. The parameter Q_0 describes the type of clouds and is, in this example, fixed to the value of 80 as it can be informed from theoretical models. The bounds of the cloud parameters are chosen to cover a wide range of possibilities: $R_{\rm clouds}$ varies between 0.003 and 1 μm and $\chi_{\rm clouds}$ varies between 10^{-15} and 10^{-3}. As with WASP-33 b, we chose a three-point thermal profile and apply the same bounds (490–1690 K). For these two cases, the full posteriors are presented in Appendix D (Figure 16) and Appendix E (Figure 17). The fitted spectrum, the chemical profiles and the TP profile are presented in Figure 11.

We find that for the two-layer hybrid scenario, all input chemical parameters except the abundance of CO can be recovered. Due to the high opacity, we retrieve weak constraints on the temperature parameters at high pressure, returning large posteriors for $T_{\rm surf}$, T_1 and the associated pressures. The cloud parameters are retrieved within the expected values. We notice a strong correlation between the clouds' particle size and their abundances.

In the full one-layer scenario, the solution provides a good fit to the observation, while the retrieved abundances for H_2O and CH_4 seem to average the real profiles. However, it appears that the temperature profile exhibit large variations, especially for pressures lower than 10^{-2} bar, where the true temperature profile is outside the retrieved 1σ temperature. The difficulty encountered by the one-layer scenario in explaining the spectrum is also confirmed by the retrieved posteriors in Appendix Figure 17 where, in particular, the temperature and pressure of point 2 are offset from the true values and are degenerate with the other parameters. We also find that the radius is not as well retrieved as in the two-layer hybrid case. In practice, the one-layer solution would be unlikely to be accepted since the retrieved temperature points tend to push toward values outside reasonable priors.

This result confirms that the isothermal assumption could lead to biases in retrievals of *JWST* and *ARIEL* (Rocchetto et al. 2016). Additionally, the mixing ratio of around 10^{-10} of H_2O in the upper atmosphere is too low to be captured by observations given the large haze opacity assumed. For this planet, the detection limit of H_2O at this altitude is around 10^{-5}, correctly interpreted by the large error bars. Also, for this example, by using a two-layer retrieval, correlations in the chemical profiles and detection of cloud layers in transit spectra could inform us about the nature of hazes and clouds.

5. Discussion

5.1. A Physically Motivated Reason to Consider Nonconstant Vertical Chemical Profiles

We have shown in the previous sections that simulated atmospheres with a two-layer chemical profile would induce spectral features that need to be properly accounted for in retrievals to avoid incorrect conclusions. However, one could ask whether such a family of chemical profiles can be found in exoplanetary atmospheres. We have already demonstrated through the cases of WASP-33 b and GJ 1214b that chemical profiles with vertical discontinuities could be important if clouds and hazes are present in the atmosphere.

Additionally, chemical simulations by Venot et al. (2012) suggest at least two typical behaviors for chemical profiles in exoplanetary atmospheres of the type HD 209458b. Some molecules of interest, such as H_2O and CO, are predicted to have a constant mixing ratios as a function of pressure. Others, like NH_3 or CH_4, are expected to vary with altitude. In the deep atmosphere (generally pressures higher than 1 bar/10^5 Pa) chemical reactions are close to their thermochemical equilibrium values. In the higher part of the atmosphere ($\sim 10^{-4}$ bar/10 Pa) photo-chemistry and disequilibrium processes may modify the overall mix by dissociation and creation of atomic species and new molecules. In addition, Moses et al. (2013) investigated the composition of hot Neptunes like GJ 436 b

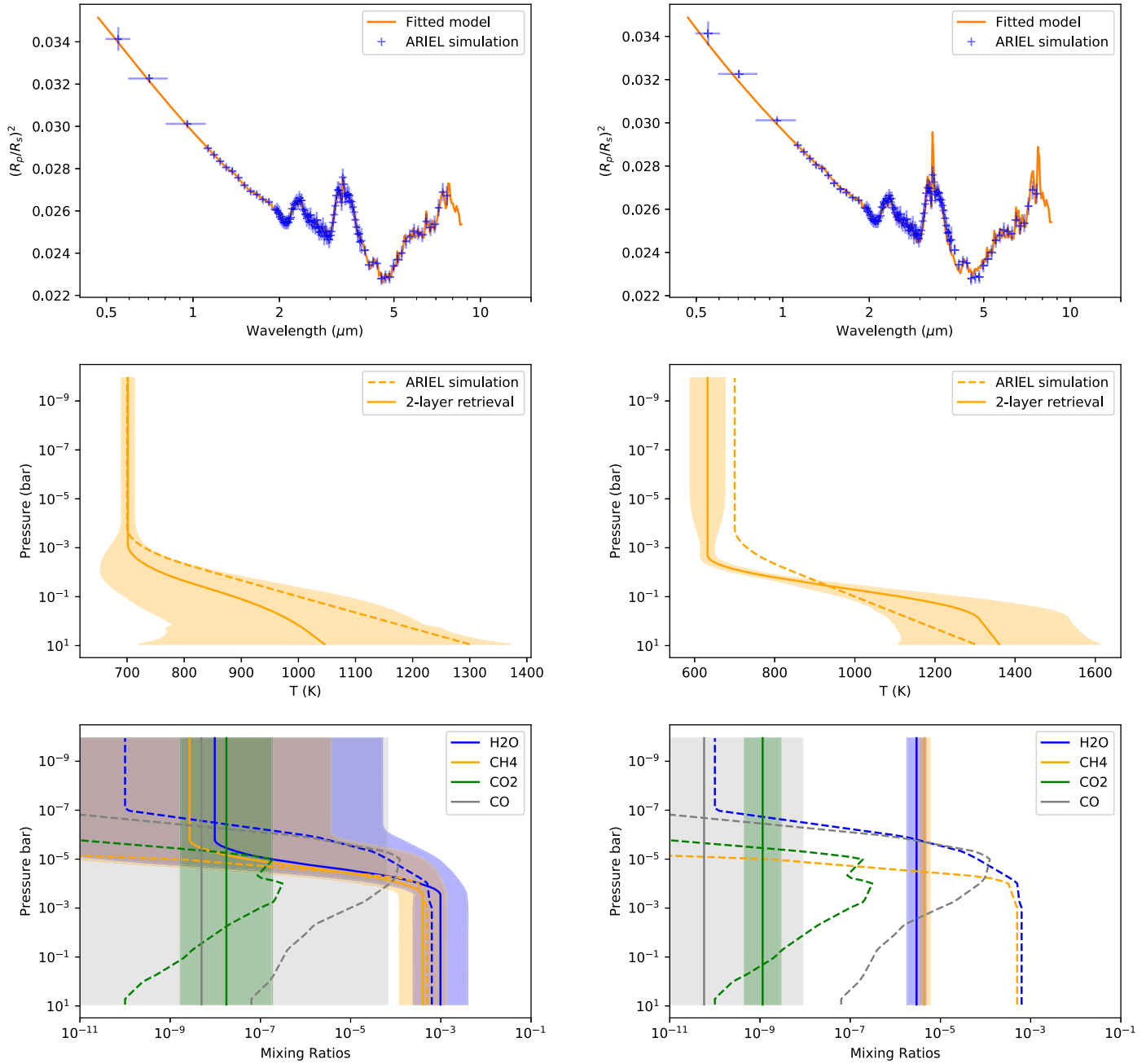

Figure 11. Results of the retrieval for a planet like GJ 1214b. Left: two-layer profile for H_2O and CH_4, while CO_2 and CO use constant profiles. Right: all molecules are retrieved with constant (one-layer profile) chemistry. Top rows: fitted spectra; middle rows: temperature profiles; and bottom rows: chemical profiles of H_2O, CH_4, CO_2, and CO. For the temperature and the chemical profiles, the dotted lines correspond to the input values. For the two-layer run we obtain $\log(E) = 736$, while for the one-layer run we get $\log(E) = 691$ ($\Delta\log(E) = 45$).

with a wide range of metallicities and the resulting chemical profiles demonstrated complex behaviors. This highlights the need for adapted retrieval techniques. These disequilibrium processes are expected to be more prominent and important in colder atmospheres (Tinetti et al. 2018).

Future space instruments should be able to probe roughly between 1 and 10^{-5} bar, depending on the composition and temperature of the atmosphere, allowing us to constrain chemical models with direct observations. This is showcased in Figure 12, where the plots illustrate the contribution functions and their wavelength dependencies for planets similar to HD 209458b, WASP-33 b, and GJ 1214b.

5.2. Should We Always Use the Two-layer Model?

The increase in complexity in chemical models must be done with care. In some cases, the introduction of additional degrees of freedom comes at the expense of model convergence, i.e., the flexibility of the retrieval should depend on the quality of the input data. This opens up the question of model selection. Indeed, should we prefer models with increased flexibility at the risk of increasing model degeneracies and overfitting, or should we prefer simpler models but returning only "acceptable" fits?

In the two-layer case, this issue can be illustrated by the retrieval of a constant input. In Section 3.1, we disabled the retrieved pressure point to ensure the convergence of the

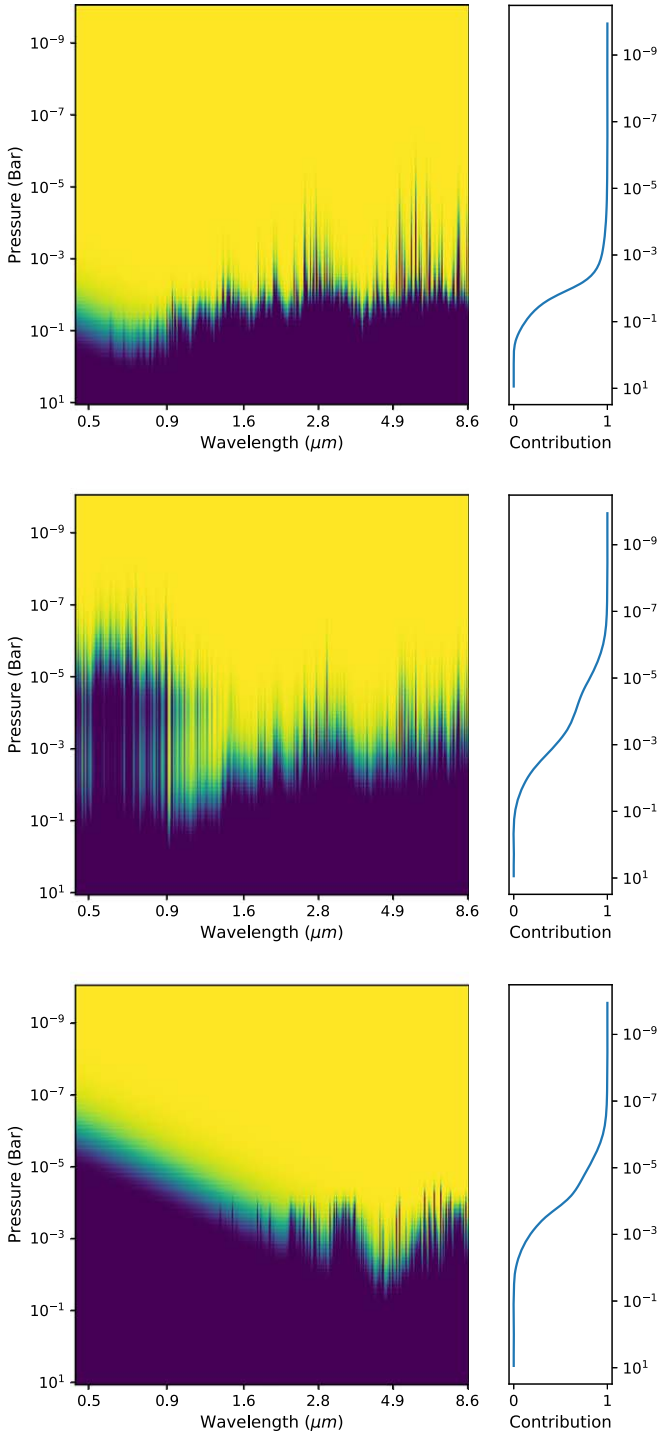

Figure 12. Opacity contribution functions for (top) a hot Jupiter (e.g., HD 209458b); (middle) an Ultra Hot-Jupiter (e.g., WASP-33 b); and (bottom) a sub-Neptune (e.g., GJ 1214b). In each plot, the left panel shows the contribution function as a function of wavelength (horizontal axis) and the pressure (vertical axis). The right panel is the same function averaged over all wavelengths. For a Hot Jupiter like HD 209458b, the pressures probed range from 1 to 10^{-4} bar. For an Ultra-Hot Jupiter of the type WASP-33 b, the contribution ranges from 10^{-1} to 10^{-7} bar. For a Mini-Neptune planet like GJ 1214b, the contribution function spans the pressures from 10^{-1} to 10^{-6} bar.

two-layer retrieval. This choice was justified by the fact that the input pressure point does not exist in constant chemical profiles, making any retrieved pressure point suitable and therefore introducing an intrinsic degeneracy. In Figure 13 the constant chemical profile used as input is here retrieved with the retrieved pressure point activated (log $P(H_2O)$). The point is, however, not well constrained and the retrieved abundances become more difficult to interpret. The posteriors are compatible with a bimodal solution peaked at pressures where observations are no longer sensitive.

This example highlights the circumstances under which the model used in the retrieval is too complex. The issue was solved previously in Figure 3 by fixing the retrieved pressure to an arbitrary value (reduction of the model complexity), illustrating that if/when the two-layer model is too complex for the data, one needs to decrease the number of free parameters and revert back to a simpler chemical parameterization. This can clearly be seen from the posterior distribution (namely the pressure point divergence).

6. Conclusion

In this paper we have assessed the possibility of constraining the abundance as a function of altitude of key chemical species present in exoplanet atmospheres. We have used simulated *JWST* and *ARIEL* transit spectra to test whether the data quality of the next generation of space-based instruments will allow for the retrieval of vertical chemical profiles. The two-layer model assumed in our paper, while still being a coarse approximation of the real case, provides an increased level of complexity and flexibility in the interpretation of the data compared to the assumption of constant abundance for each chemical species. To test the validity and usefulness of the model, we included the two-layer method in the spectral retrieval algorithm TauREx and performed the retrieval of *JWST*- and *ARIEL*-like transit spectra generated by assuming both ad hoc, simplified atmospheric examples and more realistic cases.

We found that the two-layer retrieval is able to capture accurately discontinuities in the vertical chemical profiles, which could be caused by disequilibrium processes—such as vertical mixing or photochemistry—or the presence of clouds/hazes. Our approach should therefore help the removal of the hurdles in interpreting observational constraints that have hindered the confirmation of current chemical models published in the literature. Additionally, the two-layer retrieval could help to constrain the composition of clouds and hazes by studying the correlation between the chemical changes in the gaseous phase and the pressure at which the condensed/solid phase occurs. This result is particularly important given that clouds/hazes have been detected in half of the currently available exoplanet spectra, but their composition is still elusive as it cannot be inferred directly through remote sensing measurements.

Future work will extend this analysis to eclipse spectra and explore the need for more complex vertical profiles.

This project has received funding from the European Research Council (ERC) under the European Union's Horizon 2020 research and innovation programme (grant agreement No. 758892, ExoAI), under the European Union's Seventh Framework Programme (FP7/2007-2013)/ERC grant agreement numbers 617119 (ExoLights) and the European Union's Horizon 2020 COMPET programme (grant agreement No. 776403, ExoplANETS A). Furthermore, we acknowledge funding by the Science and Technology Funding Council (STFC) grants: ST/K502406/1, ST/P000282/1, ST/P002153/1, and ST/S002634/1.

Software: TauREx (Waldmann et al. 2015a, 2015b), ArielRad (L. Mugnai et al. 2019, in preparation), Multinest (Feroz et al. 2009), Corner.py (Foreman-Mackey 2016).

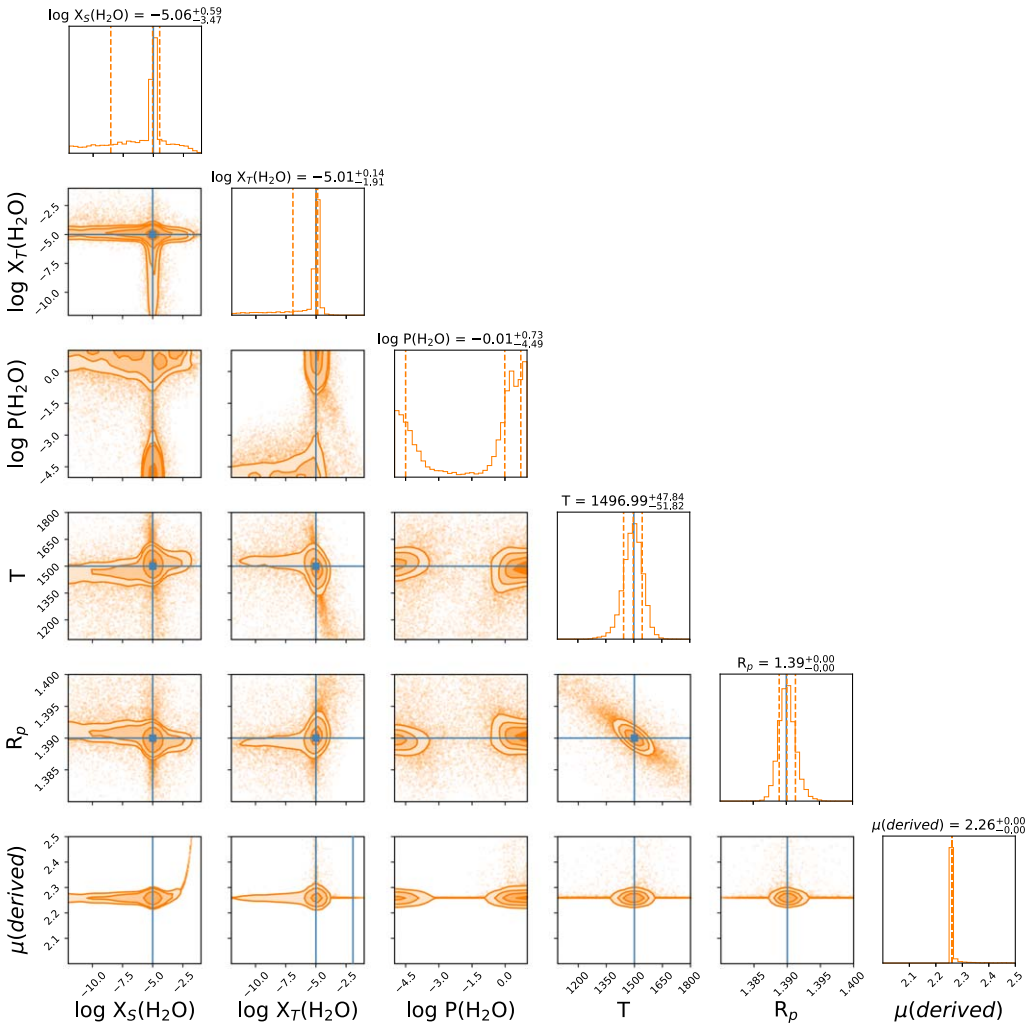

Figure 13. Posterior distribution for the retrieval of a constant H_2O input profile using the two-layer model with the retrieved pressure point activated. The model cannot converge as multiple solutions for this point exist. This solution indicates that the number of free parameters is too high and we need to revert to a simpler retrieval.

Appendix A
Planet's Parameters Used for the Forward Models

Table 3 presents the parameters used in our forward models for the three types of planets: a hot-Jupiter type HD 209458b (Stassun et al. 2017), an ultra hot-Jupiter type WASP-33 b (Stassun et al. 2017), and a sub-Neptune type GJ 1214b (Harpsøe et al. 2013):

Table 3
Planet's Parameters Used for the Forward Models

Parameters	Hot Jupiter	Ultra Hot Jupiter	Sub Neptune
$R_s(R_{\rm Sun})$	1.19	1.55	0.216
$T_s(K)$	6091	7308	3026
$R_p(R_{\rm Jupiter})$	1.39	1.6	0.254
$M_p(M_{\rm Jupiter})$	0.73	1.17	0.0197

Appendix B

Posteriors of Retrievals for a Planet with an Inverted H_2O Chemical Profile Using Constant and Two-layer Chemical Models. Figure 14 presents the posterior distributions for two retrievals (one-layer and two-layer models) of a hot-jupiter, which presents variation of abundances with altitude.

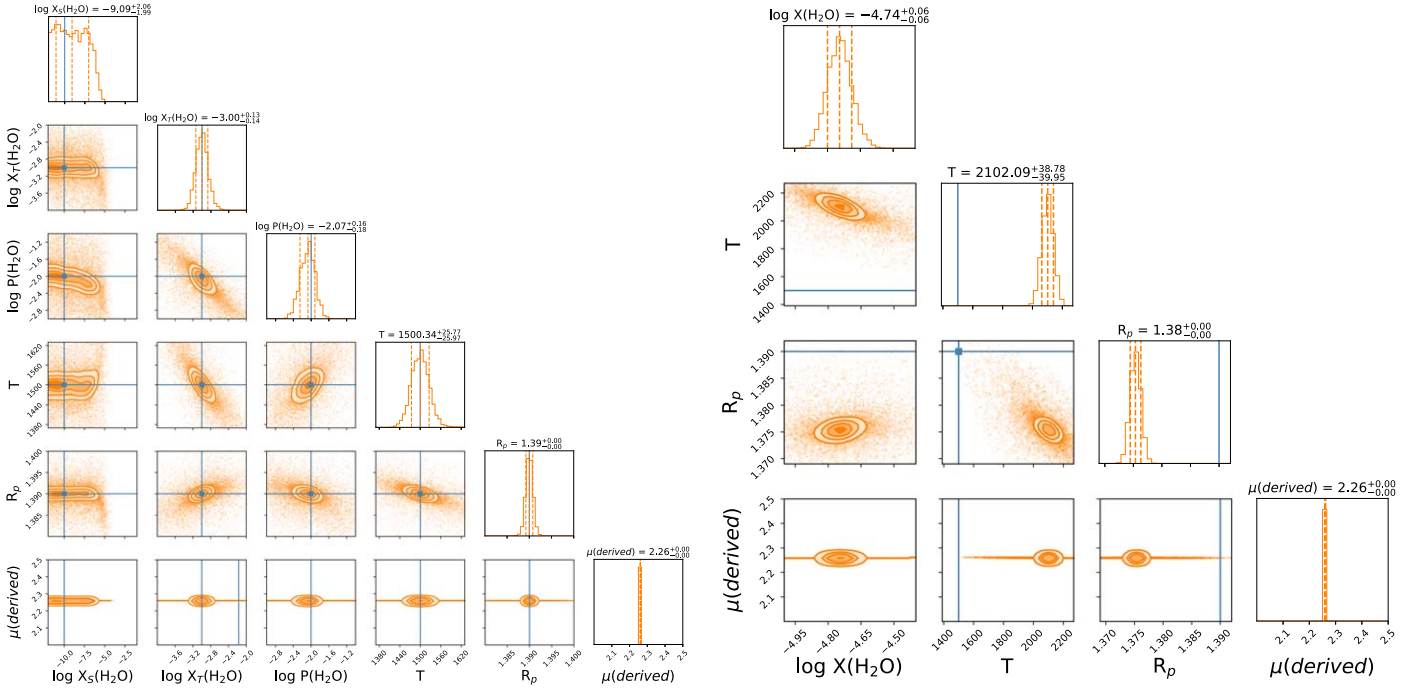

Figure 14. Posteriors of the two-layer retrieval (left) and the constant retrieval (right) for a simulated *ARIEL* observation of a planet with an inverted H_2O profile. The top layer contains $X_T(H_2O) = 10^{-3}$ for pressures lower than $_{P_t}(H2O) = 10^{-2}$ bar and the surface layer is depleted with a mixing ratio of only $X_S(H_2O) = 10^{-10}$.

Appendix C

Posteriors Distribution for the Retrieval of WASP-33 b. The posterior distribution for a ultra-hot-jupiter type planet is shown in Figure 15. In the input model, the planet presents a TiO layer at the top of the atmosphere.

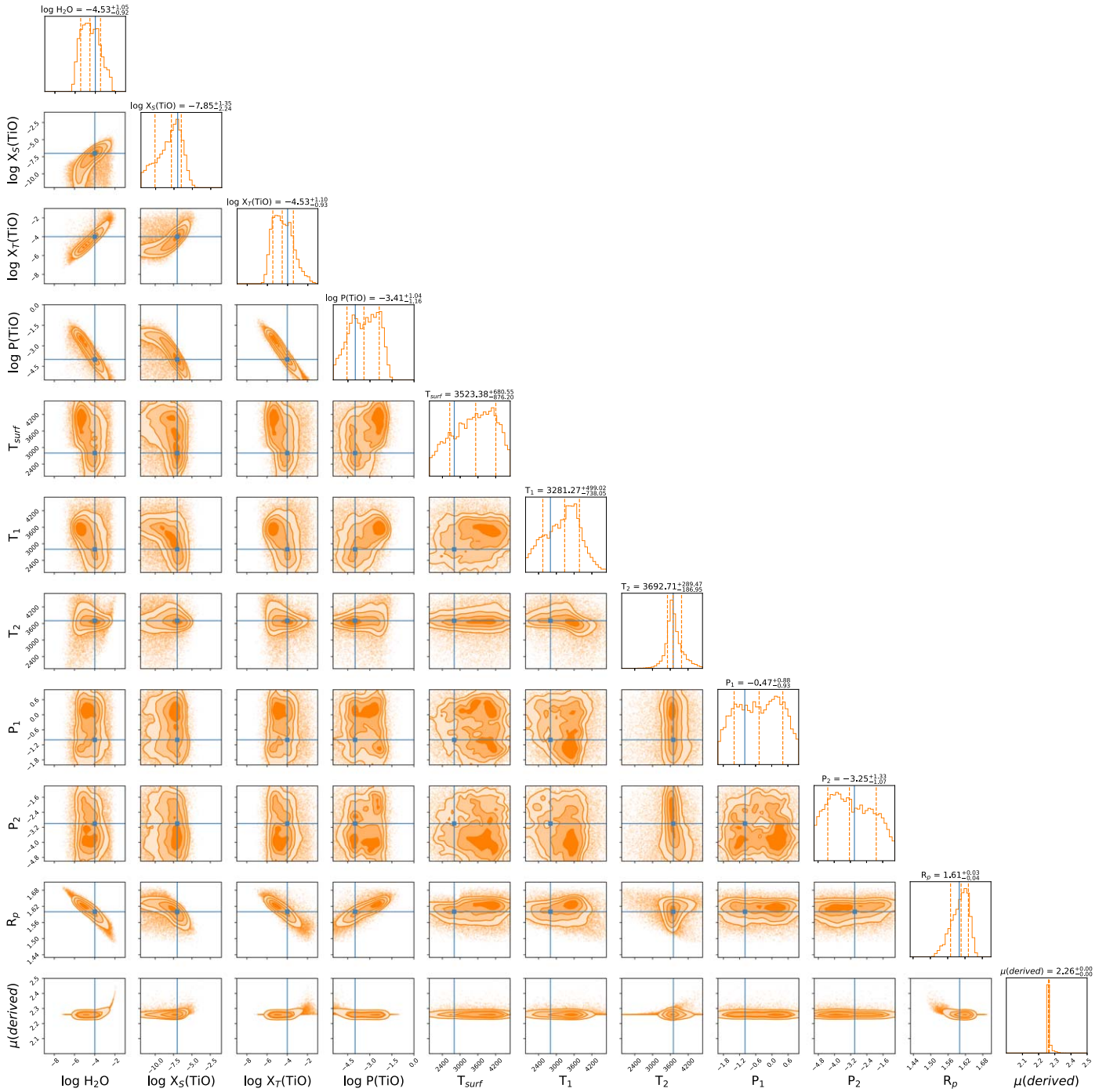

Figure 15. Posteriors distribution for the retrieval of WASP-33 b. The planet presents constant H_2O abundance and a TiO 2-layer profile with a large abundance in the upper atmosphere.

Appendix D

Posteriors Distribution for the Retrieval of GJ 1214b with Two-layer Profiles for H_2O and CH_4 and Constant Profiles for CO_2 and CO. In Figure 16, we show the retrieved posteriors of our two-layer model for the sub-neptune type planet. The input model includes disequilibrium chemistry, temperature variations, and a cloud parametrisation.

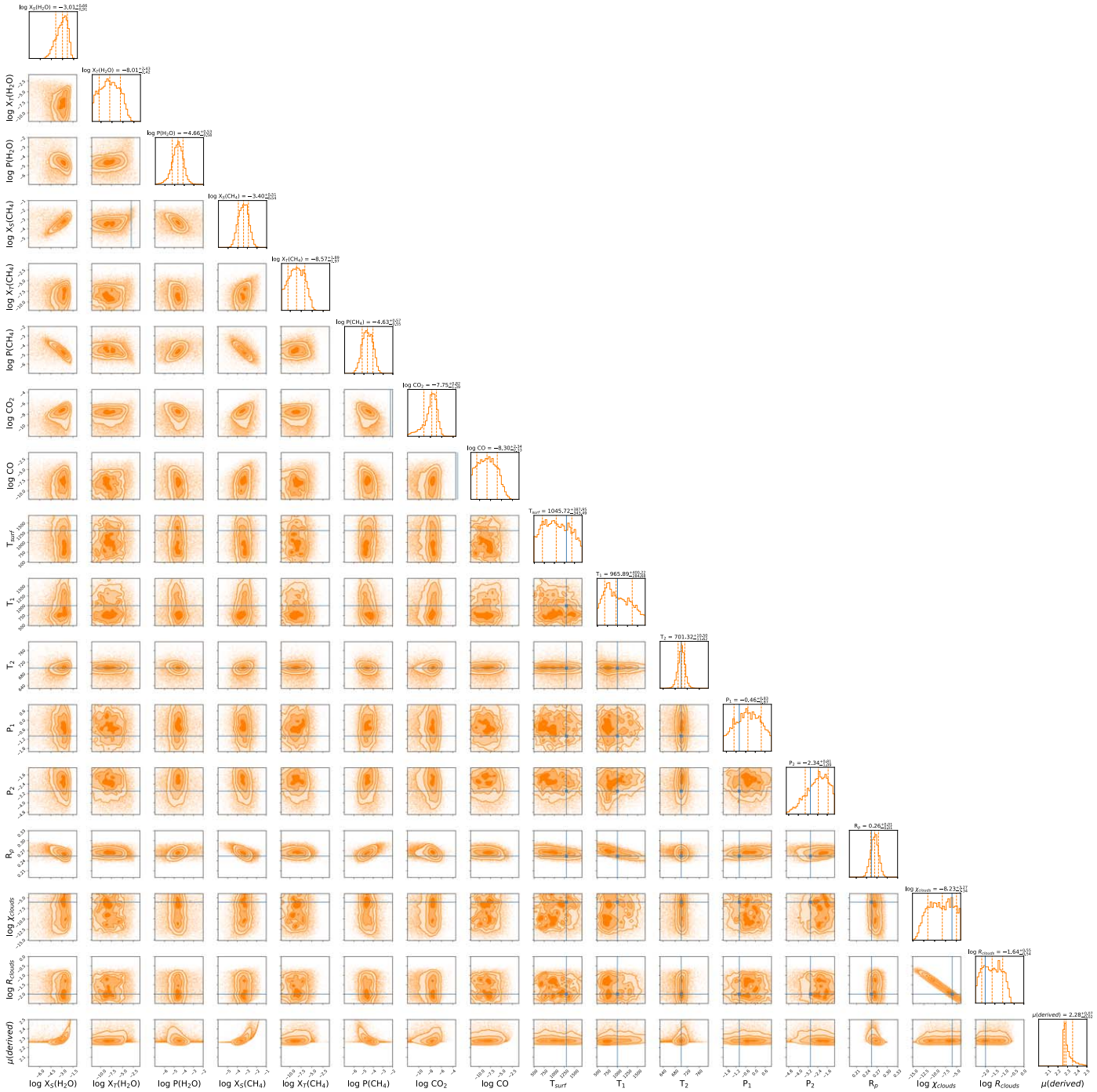

Figure 16. Posteriors distribution for the retrieval of GJ 1214b with hydrocarbon hazes. The planet is retrieved using two-layer for H_2O and CH_4. Hydrocarbon hazes are added in the atmosphere to simulate the irradiation of CH_4.

Appendix E

Posteriors Distribution for the Retrieval of GJ 1214b in the Case of Constant Chemical Profiles. In Figure 17, we show the retrieved posteriors of the standard one-layer model for the sub-neptune type planet. The input model includes disequilibrium chemistry, temperature variations, and a cloud parametrisation. The retrieved posteriors present degenerate solutions and odd correlations.

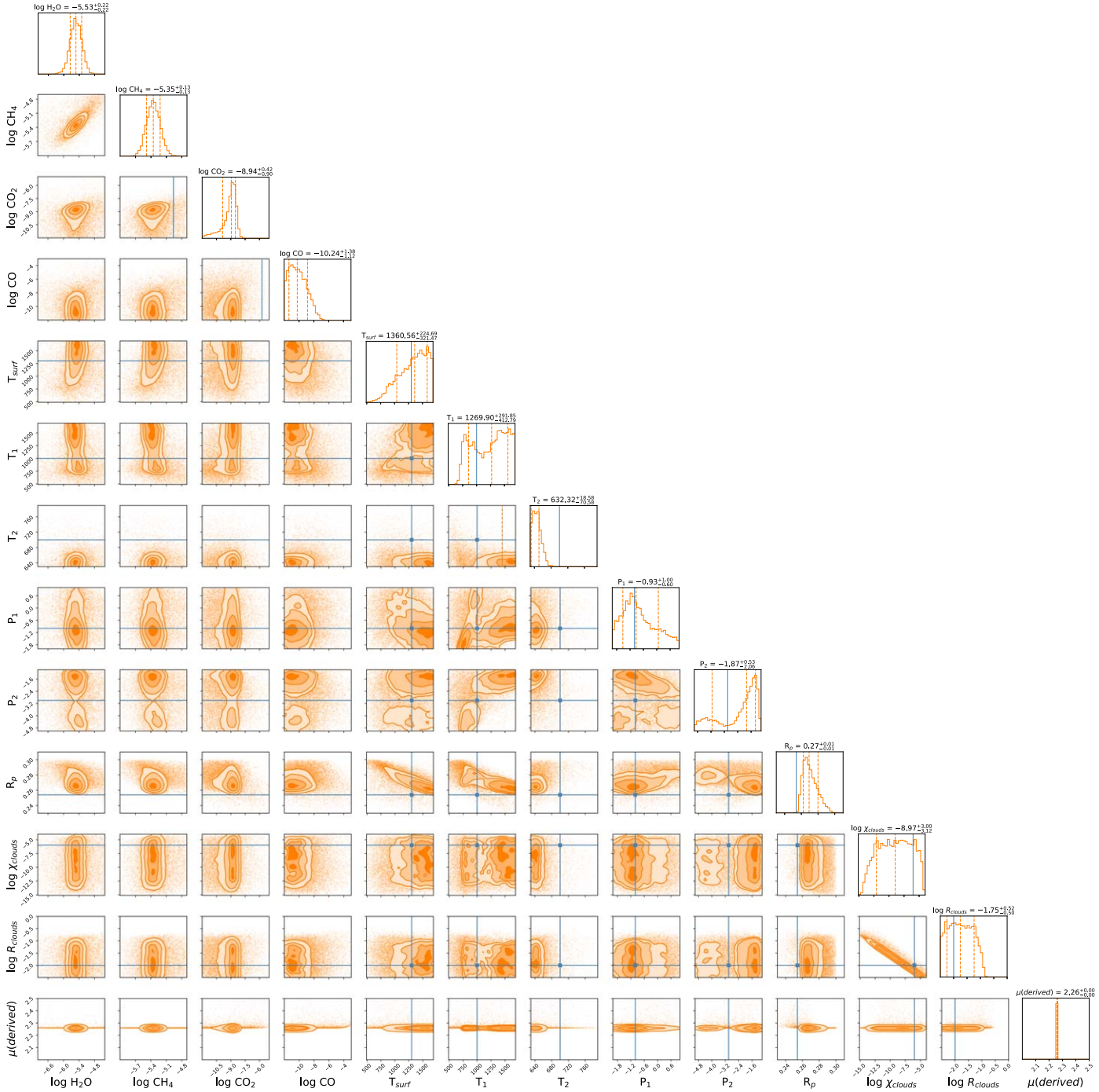

Figure 17. Posteriors distribution for the retrieval of GJ 1214b with hydrocarbon hazes. The planet is retrieved using constant chemistry for all molecules.

ORCID iDs

Q. Changeat https://orcid.org/0000-0001-6516-4493
B. Edwards https://orcid.org/0000-0002-5494-3237
I. P. Waldmann https://orcid.org/0000-0002-4205-5267
G. Tinetti https://orcid.org/0000-0001-6058-6654

References

Abel, M., Frommhold, L., Li, X., & Hunt, K. L. 2011, JPCA, 115, 6805
Abel, M., Frommhold, L., Li, X., & Hunt, K. L. 2012, JChPh, 136, 044319
Agúndez, M., Parmentier, V., Venot, O., Hersant, F., & Selsis, F. 2014, A&A, 564, A73
Barton, E. J., Hill, C., Yurchenko, S. N., et al. 2017, JQSRT, 187, 453
Bean, J. L., Stevenson, K. B., Batalha, N. M., et al. 2018, PASP, 130, 114402
Brandl, B. R., Absil, O., Agócs, T., et al. 2018, Proc. SPIE, 10702, 107021U
Cox, A. N. 2015, Allenas Astrophysical Quantities (Berlin: Springer)
Cubillos, P., Blecic, J., Harrington, J., et al. 2016, BART: Bayesian Atmospheric Radiative Transfer Fitting Code, Astrophysics Source Code Library, ascl:1608.004
Edwards, B., Mugnai, L., Tinetti, G., Pascale, E., & Sarkar, S. 2019a, AJ, 157, 242
Edwards, B., Rice, M., Zingales, T., et al. 2019b, ExA, 47, 29
Evans, T. M., Sing, D. K., Kataria, T., et al. 2017, Natur, 548, 58
Feng, Y. K., Robinson, T. D., Fortney, J. J., et al. 2018, AJ, 155, 200
Feroz, F., Hobson, M. P., & Bridges, M. 2009, MNRAS, 398, 1601
Fletcher, L. N., Gustafsson, M., & Orton, G. S. 2018, ApJS, 235, 24
Foreman-Mackey, D. 2016, JOSS, 1, 24
Fortney, J. J., Lodders, K., Marley, M. S., & Freedman, R. S. 2008, ApJ, 678, 1419
Gandhi, S., & Madhusudhan, N. 2018, MNRAS, 474, 271
Gordon, I., Rothman, L. S., Wilzewski, J. S., et al. 2016, AAS/DPS Meeting, 48, 421.13
Goyal, J. M., Mayne, N., Sing, D. K., et al. 2018, MNRAS, 474, 5158
Guillot, T. 2010, A&A, 520, A27
Harpsøe, K. B. W., Hardis, S., Hinse, T. C., et al. 2013, A&A, 549, A10
Haynes, K., Mandell, A. M., Madhusudhan, N., Deming, D., & Knutson, H. 2015, ApJ, 806, 146
Heng, K., Mendonça, J. M., & Lee, J.-M. 2014, ApJS, 215, 4
Hill, C., Yurchenko, S. N., & Tennyson, J. 2013, Icar, 226, 1673
Irwin, P. G. J., Teanby, N. A., de Kok, R., et al. 2008, JQSRT, 109, 1136
Jeffreys, H. 1998, The Theory of Probability (Oxford: Oxford Univ. Press)
Kass, R. E., & Raftery, A. E. 1995, J. Am. Stat. Assoc., 90, 773
Kreidberg, L., Bean, J. L., Désert, J.-M., et al. 2014, Natur, 505, 69
Lavie, B., Mendonça, J. M., Mordasini, C., et al. 2017, AJ, 154, 91
Lee, J.-M., Heng, K., & Irwin, P. G. J. 2013, ApJ, 778, 97
Li, G., Gordon, I. E., Rothman, L. S., et al. 2015, ApJS, 216, 15
Line, M. R., Wolf, A. S., Zhang, X., et al. 2013, ApJ, 775, 137
MacDonald, R. J., & Madhusudhan, N. 2017, MNRAS, 469, 1979
Madhusudhan, N., & Seager, S. 2009, ApJ, 707, 24
Malik, M., Grosheintz, L., Mendonça, J. M., et al. 2017, AJ, 153, 56
Miller-Ricci Kempton, E., Zahnle, K., & Fortney, J. J. 2012, ApJ, 745, 3
Morley, C. V., Fortney, J. J., Kempton, E. M.-R., et al. 2013, ApJ, 775, 33
Moses, J. I., Line, M. R., Visscher, C., et al. 2013, ApJ, 777, 34
Nugroho, S. K., Kawahara, H., Masuda, K., et al. 2017, AJ, 154, 221
Pinhas, A., Madhusudhan, N., Gandhi, S., & MacDonald, R. 2019, MNRAS, 482, 1485
Polyansky, O. L., Kyuberis, A. A., Zobov, N. F., et al. 2018, MNRAS, 480, 2597
Rocchetto, M., Waldmann, I. P., Venot, O., Lagage, P. O., & Tinetti, G. 2016, ApJ, 833, 120
Rothman, L., Gordon, I., Barber, R., et al. 2010, JQSRT, 111, 2139
Rothman, L. S., & Gordon, I. E. 2014, 13th Int. HITRAN Conf. (Cambridge, MA), 2014
Schwenke, D. W. 1998, FaDi, 109, 321
Spiegel, D. S., Silverio, K., & Burrows, A. 2009, ApJ, 699, 1487
Stassun, K. G., Collins, K. A., & Gaudi, B. S. 2017, AJ, 153, 136
Tennyson, J., Yurchenko, S. N., Al-Refaie, A. F., et al. 2016, JMoSp, 327, 73
Terrile, R. J., Fink, W., Huntsberger, T., et al. 2005, BAAS, 37, 31.19
Tinetti, G., Drossart, P., Eccleston, P., et al. 2018, ExA, 46, 135
Tsiaras, A., Waldmann, I. P., Zingales, T., et al. 2018, AJ, 155, 156
Venot, O., Hébrard, E., Agúndez, M., et al. 2012, A&A, 546, A43
Waldmann, I. P., Rocchetto, M., Tinetti, G., et al. 2015a, ApJ, 813, 13
Waldmann, I. P., Tinetti, G., Rocchetto, M., et al. 2015b, ApJ, 802, 107
Yurchenko, S. N., & Tennyson, J. 2014, MNRAS, 440, 1649